From the Department for Pathophysiology, Infectiology and Immunology
of the University of Medicine of Vienna

Institute for Hygiene and Applied Immunology
(Head: Assoc. Prof. Johannes Huppa, PhD)

Assessing synaptic TCR-pMHC binding kinetics via single molecule FRET measurements and single dye tracing

Bachelor thesis

University of Veterinary Medicine Vienna

Jakob Lichtblau

Vienna, July 2022

Supervisor: Univ.-Prof. Dr. rer. nat. Armin Saalmüller

Reviewer: Assistant Prof. Dipl.-Ing. Dr. techn. Eva Sevcsik

Table of Contents

1. Introduction

1.1. Prologue

T lymphocytes (T cells) play an essential role in the adaptive pathway of our immune response to pathogens. In the past 30 years, much effort has been put into characterizing T-cell responses to pathogens and tumors, as well as investigating molecular mechanisms behind the intercellular signaling pathways T cells require to function. A critical step in the T-cell-mediated immune responses is T-cell activation after recognition of non-endogenous peptides on the surface of antigen presenting cells (APCs) by means of T-cell antigen receptors (TCRs). Peptides that stimulate T cells (from here on referred to as antigens) can be derived from different sources, such as larger microbial proteins and are processed by APCs prior to presentation. For the T cell to be able to recognize an antigen and initiate an immune response, the antigen must be linearized and bound to a major histocompatibility complex surface protein of class I or II (MHCI or MHCII) (Murphy und Weaver 2016). TCRs have evolved to recognize a virtually infinite number of antigens by somatic recombination of variable (V), diversity (D) and joining (J) segments (Litman et al. 2010). Every T cell expresses a unique TCR and is therefore equipped to recognize a specific antigen.

The class of MHC that can be recognized by a given T cell is in part determined by the type of coreceptor or cluster of differentiation glycoprotein (CD4 or CD8) expressed on the T cell surface. CD4/CD8 antigens interact with the peptide-bound MHC (pMHC) and this engagement is required to elicit the full effect of T-cell activation (Murphy und Weaver 2016). CD4 carrying cells ($CD4^+$ cells) generally recognize pMHCIIs, while $CD8^+$ cells become activated by pMHCIs. After antigen contact and subsequent activation, $CD4^+$ T helper cells (T_H cells) secrete the cytokines interleukin-2 (IL-2) and tumor necrosis factor-α (TNFα) among others, which act directly on the conjugated APC (Huppa und Davis 2003). $CD8^+$ cells are more directly involved in target cell killing by secretion of perforins and granzymes (Harty et al. 2000). When first encountering a stimulatory antigen, naïve T cells are activated and start to proliferate, essentially creating copies of themselves with the same antigen specificity. All newly divided and differentiated T cells, termed effector T cells, can exert their functions immediately and without further differentiation. This allows them to eliminate pathogens, as well as certain tumor cells, effectively and efficiently (Murphy und Weaver 2016). After the source of the antigenic stimulus is neutralized, most cells of the expanded T-cell population undergo apoptosis, with only a few remaining, which become long-lived memory T cells.

Afterwards, repeated exposure to the same antigen leads to a faster response since there is a surviving stock of T cells specific to that antigen (Ahmed und Gray 1996). Furthermore, the response of memory T cells is characterized by 10 fold higher cytokine production than that of naïve T cells (Huang et al. 2013).

1.2. Molecular mechanisms of T cell activation and the immunological synapse

Intercellular T-cell signaling is mediated by the establishment of an immunological synapse (IS), which has previously been defined as a flat interface between the T cell and an APC (Huppa und Davis 2003). Prior to establishment of an IS, T cells actively recruit specific membrane- and cytoskeleton-associated molecules (such as TCRs, gangliosides and the microtubule organizing center MTOC) to the contact site, a process referred to as capping or polarization (Kupfer und Dennert 1984, Spiegel et al. 1984). Immunological synapses are only formed after sufficient TCR stimulation by activating pMHCs and are a prerequisite for the realization of the T cell's full effector potential (Huppa et al. 2003, Huppa und Davis 2003). Surface proteins within the immunological synapse are not homogeneously distributed, but form clusters with TCRs in the center, surrounded by a ring of adhesion molecules (Grakoui et al. 1999). The central TCR-cluster is called central supra-molecular activation complex (cSMAC), while the peripheral ring is referred to as pSMAC. (Huppa und Davis 2003). Transport of surface proteins to form these structures is mediated by active rearrangement of the cytoskeleton, namely actin filaments and microtubules (Campi et al. 2005).

cSMAC formation takes place at later stages of T-cell engagement, several minutes after the first antigen contact and is therefore not a requirement for T-cell activation or T-cell effector function (Purbhoo et al. 2004). TCR microclusters have also been shown to assemble much earlier than the establishment of the fully formed immunological synapse (Campi et al. 2005). It has been reasoned that one of the purposes of the immunological synapse is improving cell adhesion, which is in large part mediated by the integrin LFA-1 on the T cell, which provides a firm connection via its ligand ICAM-1 on the surface of the APC (Grakoui et al. 1999). Another benefit of the immunological synapse is more efficient presentation of co-stimulatory molecules, such as the cluster of differentiation protein 80 (CD80, also called B7-1), which are required for the full effect of T-cell activation (Tseng et al. 2008, Chen und Flies 2013).

TCRs are a heterodimer composed of an α- and a β-polypeptide chain, which both possess a variable and an immunoglobulin-like (Ig-like) domain (Garcia et al. 1996) and which are non-

covalently associated with the invariant chains of the CD3 complex, namely the CD3γ, δ- and ε-chains and the disulfide-bonded CD3ζ-homodimer (Meuer et al. 1983). The intracellular part of the CD3 complex contains immunoreceptor tyrosine-based activation motifs (ITAMs), which become phosphorylated by protein tyrosine kinases after TCR-ligand binding. ITAM phosphorylation is carried out by the CD4/CD8-associated Src-family kinase Lck. CD4/CD8 coreceptors therefore support T-cell activation by recruiting this kinase to ligand-engaged TCRs by binding to the same pMHC (Murphy und Weaver 2016). ITAM phosphorylation constitutes one of the first steps, if not the first step, within the canonical T-cell activation cascade, which culminates via the intracellular release of calcium in the release of cytokines and for CTLs also target cell lysis. However, the exact molecular mechanisms underlying the signal transfer across the plasma membrane after antigen binding to a TCRαβ-CD3 complex are still a matter of debate (reviewed in van der Merwe und Dushek 2011).

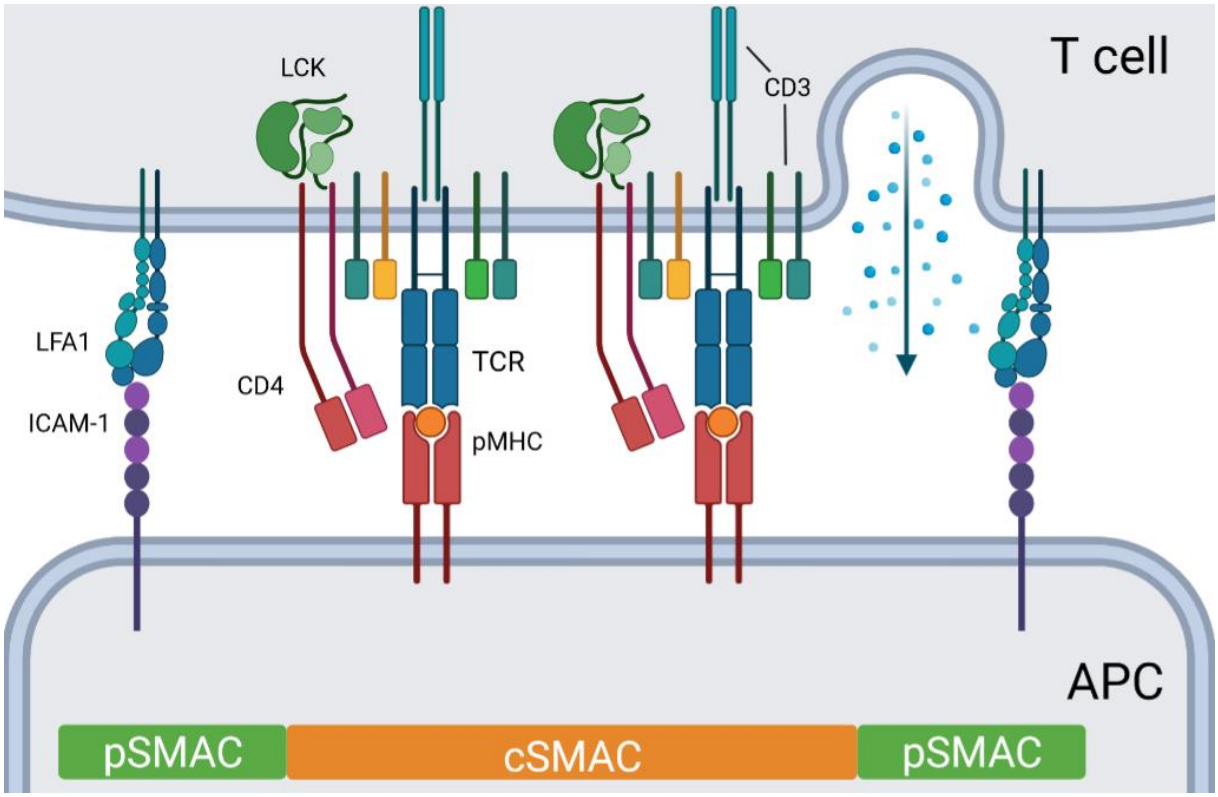

Figure 1: The immunological synapse
Schematic of an immunological synapse with cSMAC and pSMAC. Cell adhesion is mediated by LFA-1 – ICAM-1 interactions. After TCR – pMHC binding, T-cell activation leads to cytokine release into the synaptic cleft. (Created with BioRender.com)

1.3. A live-cell imaging technique utilizing FRET to investigate the immunological synapse

Recently, emerging imaging techniques for investigation of the immunological synapse have allowed researchers to measure synaptic binding kinetics of TCR – pMHC interactions *in situ*. One such method, established by Huppa et al., is a non-invasive live cell imaging approach based on Förster resonance energy transfer (FRET), which allows for detection and quantification of single molecule binding events (Huppa et al. 2010, Axmann et al. 2015). FRET is the process of energy transfer from an excited donor fluorophore to an acceptor fluorophore, a quantum-mechanical phenomenon which can be taken advantage of to measure protein-protein interactions if the interaction partners are labeled with the respective fluorophores (Förster 1948, Berney und Danuser 2003). FRET efficiency (the fraction of total energy transferred) is highly dependent on the distance between fluorophores, dropping at rates that are proportional to the inverse of the sixth power of the distance. The distance where efficiency is equal to 50 % (also termed the Förster radius) depends on the employed fluorophores and has to be accounted for when choosing a FRET pair.

In their study, Huppa et al. labeled TCRs on live 5c.c7 TCR transgenic T cells decorated with a Cy3 conjugated H57 anti-TCRβ antibody single chain fragment (H57 scF_V). They employed protein-functionalized, glass-supported and laterally mobile lipid bilayers (SLBs) equipped with ICAM-1, the costimulatory molecule B7-1 and antigenic pMHCII-molecules, which were conjugated to the fluorophore Cy5. Stained T cells were confronted with the SLB, which allowed Cy3-scF_V-bound TCRs to interact with pMHC-Cy5. It is only in the bound state that the distance between the corresponding FRET fluorophores allows for measurable FRET to occur. The assay allows for determination of the equilibrium constant K_d of TCR – pMHC interactions within the IS, the direct measurement of the off-rate (k_{off}) and following the law of mass action with these two values the numerical calculation of the on-rate (k_{on}). For determination of K_d, the FRET yield needs to be determined, e.g. by means of measuring the FRET donor recovery after acceptor photobleaching (DRAAPB; see Figure 2). This value can then be applied to calculate the percentage of synaptic TCRs engaged by pMHCs. Off-rates on the other hand are calculated with interaction lifetime measurements of single molecule binding events, employing low pMHC densities on the SLB (single molecule FRET, or smFRET). For smFRET measurements, donor fluorophores are excited and single molecule acceptor fluorophore emissions are recorded over time, allowing for quantification of single TCR – pMHC binding interactions.

Interestingly, Huppa et al. concluded that TCR - pMHC binding interactions were accelerated in *in situ* smFRET measurements, when compared to results obtained by *in vitro* surface plasmon resonance (SPR) measurements. Binding half-lives *in situ* were reported to be in the range of only several hundred milliseconds to a few seconds.

1.4. The concept of serial rebinding

The transient nature of TCR – pMHC interactions, especially when measured *in situ*, opens up new questions regarding the mechanism by which T cells differentiate between endogenous and non-endogenous antigens (reviewed in Huppa und Davis 2013). In the process of antigen recognition, T cells show remarkable sensitivity. Responses occur even after single binding events and fewer than ten TCR-ligands are needed for optimal cytokine production, lineage commitment and target cell killing (Irvine et al. 2002, Purbhoo et al. 2004, Huang et al. 2013). In addition, T cells also need to establish via their TCRs a high level of specificity and sensitivity, since APC surfaces display endogenous in much greater numbers than stimulatory pMHCs (Irvine et al. 2002) and since errors would have fatal consequences. When considering the low affinity and short lifetimes of TCR – pMHC interactions, the question arises how T cells can achieve this high sensitivity and specificity.

While this phenomenon is yet poorly understood, some studies have suggested that serial binding of single antigenic pMHCs to many TCRs may be critical for T-cell activation (Valitutti et al. 1995). In a recent study, Hellmeier et al. investigated the efficiency of TCR – ligand-binding regarding T-cell activation by employing DNA-origami platforms on an SLB serving as APC surrogate, which allowed them to regulate the spacing between single TCR ligands (Hellmeier et al. 2021). While high affinity ligands with slow dissociation rates (in this case TCR-reactive H57 scF_Vs) required at least two simultaneous binding events within a distance of 20 nm for efficient activation, endogenous pMHCs with higher off-rates effectively stimulated T cells as well isolated single molecule entities. One explanation for this behavior could be sequential rebinding of low-affinity ligands, facilitated by higher off-rates, which may allow pMHCs to “jump” from one TCR to the next. TCR-reactive antibodies on the other hand can be expected to stay bound their TCR-targets for many minutes to hours, impeding possible rebinding. Overall, these results imply that spatial arrangement of TCR molecules on the T cell within microclusters could be a determining factor of TCR proximal signaling, especially in the wake of engaging physiological ligands, since this might increase chances of rebinding events taking place.

To test this hypothesis, we applied two different minimally invasive live-cell imaging methods with high spatiotemporal resolution in the millisecond and nanometer range. Both methods allowed us to visualize and quantitate single molecule binding events between TCRs on T cells and pMHCs on a biomimetic SLB *in situ*. SLBs were functionalized with the adhesion factor ICAM-1, the costimulatory peptide B7-1 and stimulatory pMHCs. T cells were transgenic for the 5c.c7 TCR, which is specific for the moth cytochrome C peptide (MCC). The cells were confronted with the pMHCII molecule I-E^k complexed with either MCC, or the higher affinity agonist peptide 2b4_5CC7_2. By comparing the results obtained with both methods, our goal was to verify whether serial rebinding constitutes a critical event for sensitized recognition of stimulatory pMHCs by TCRs.

2. Methods

2.1. Preparation of planar glass-supported lipid bilayers

1-palmitoyl-2-oleoyl-sn-glycero-3-phosphocholine (POPC) was mixed with 1,2-dioleoyl-*sn*-glycero-3-[(N-(5-amino-1-carboxypentyl) iminodiacetic acid) succinyl] (nickel salt) (Ni-DGS NTA, both Avanti polar lipids, UK) in chloroform (Merck, Germany). The solution was vacuum-dried in a desiccator overnight, resuspended in 1x PBS and sonicated in a water bath sonicator (Q700, QSonica, USA) at 120-170 W under Nitrogen to create a solution of unilamellar lipid vesicles. Glass-slides (22 mm x 64 mm and 24 mm x 50 mm, VWR, Austria) were decontaminated with a plasma cleaner (Diener electronic, Germany) for 15-20 min and then glued to the bottom of 8- or 16-well LabTek-chambers (Thermo Fisher Scientific, USA) using dental imprint silicon putty (Picodent twinsil 22, Picodent, Germany). After drying for 20 min, 50 µl of the lipid solution was added per well. For single molecule experiments and bulk FRET imaging under conditions of low abundance fluorescence-tagging, the lipid solution contained 98 % POPC and 2 % Ni-DGS NTA. For bulk FRET experiments involving high abundance fluorescence staining, a solution containing 5 % Ni-DGS NTA was used instead. Before use, lipid solutions were diluted 1:15 with 1x PBS and filtered using a 0.22 µm PVDF filter (Merck). Chambers were left to incubate for 20 min at room temperature and then rinsed with 15 ml 1x PBS per well. Proteins were diluted in PBS to the desired concentrations and centrifuged at $1.7*10^4$ g at 4 °C. ICAM-1 and B7 were added at 0.04 µl/well and 0.02 µl/well respectively. Concentrations of I-E^k ranged from 0.25 ng per well for single molecule tracking experiments to 200 ng per well for bulk FRET and fluorophore lifetime experiments. 50 µl of the supernatant was added to each well for 60-90 min at room temperature in the dark and after confirmation of sufficient fluorophore density at the microscope rinsed again with PBS. Before imaging, the PBS in each well was exchanged for an imaging buffer (IB), consisting of Hank's Balanced Salt Solution (HBSS, Thermo Fisher Scientific) supplemented with ovalbumin (0.35 mg/ml; Merck) and 2 mM $CaCl_2$ and $MgCl_2$ (Merck).

2.2. Microscopy

Microscopy experiments were performed on an Eclipse Ti-E inverted microscope (Nikon, Netherlands) with a 100x oil objective (SR Apo TIRF, NA=1.49; Nikon) supporting TIRF-illumination given its high aperture. Diode lasers with the wavelengths 532 nm and 642 nm

(both Coherent, USA) were used for laser excitation. The laser lines were equipped with cleanup filters matching the used wavelengths (Chroma, USA). In addition, we employed a xenon lamp (Lambda Ls lamp, Sutter Instrument Company, USA), equipped with a filter wheel (Sutter Instrument Company) in the excitation path with the following filters installed: 340/26, 387/11, 370/36, 474/27, 554/23, and 635/18 (all Chroma). On the emission site, we used a second filter wheel (Sutter Instrument Company) with the following emission bandpass filters installed: ET450/50, ET510/20, ET525/50, ET605/52, ET700/75 (all Chroma). For fluorescence microscopy we used the beam splitter cube zt405/488/561/647rpc and for interference reflection microscopy (IRM), we used the beam splitter zt405/514/635rpc. Microscopy was performed in epifluorescence and total internal reflection fluorescence (TIRF) configurations.

For FRET experiments, the emission image splitter Optosplit II (Cairn Research, UK) was used to separate the emission light into two spectral channels by use of a beam splitter (ZT640rdc, Chroma) and corresponding emission bandpass filters (ET575/50 and ET650LP, both Chroma). For IRM, we used the Fura-2 cube and a Cy3 (605/52) emission filter The microscope was covered with a box connected to an incubation system (Heating Unit 2000, Pecon, Germany), controlled by a temperature control system (TempController 2000-1, Pecon), allowing for regulation and monitoring of temperature. Images were taken with a backside-illuminated EM-CCD camera (Andor iXon Ultra 897, Oxford Instruments, UK). Hardware components were controlled with the microscopy automation and image analysis software Metamorph (Molecular Devices, USA) over an 8 channel DAQ-card (National Instruments, USA).

2.3. Tissue culture

Murine T-cell medium (mTCM) was prepared by supplementing 1x Roswell Park Memorial Institute (RPMI) 1640 Media with 10 % FCS (Biowest, France), 1x Penstrep (Penicillin/Streptomycin solution, Thermo Fisher Scientific), 2 mM L-Glutamine (Thermo Fisher Scientific), 1 mM sodium pyruvate (Thermo Fisher Scientific), 1x non-essential amino acids (NEAA mixture, Lonza, Switzerland), 50 µM β-mercaptoethanol (Thermo Fisher Scientific). Primary $CD4^+$ T cells were isolated from the spleen and lymph nodes of 5c.c7 TCR-transgenic mice by use of a 70 µm cell strainer (Sarstedt, Germany) and suspended in 6 ml medium. The cells were then centrifuged at 350 g for 5 minutes and resuspended in 2 ml red blood cell lysis buffer (Merck) for 3 – 4 minutes, after which 20 ml medium was added and the cells were

centrifuged again. The pellet was resuspended, cells were counted and set at a concentration of 7.5 x 10^6 cells per ml medium. Then, 1 ml of the cell-containing medium was transferred into each well of a 24-well cell culture plate (Greiner Bio-One, Austria) and supplemented with 0.5 µM C18 reverse-phase HPLC-purified MCC peptide (sequence: ANERADLIAYLKQATK, T cell epitope underlined; Elim Biopharmaceuticals, USA). The cells were then incubated for seven days at 37 °C and 5 % CO_2. On day two, cells were stimulated with 50 U/ml IL-2 (Thermo Fisher Scientific) and 1 ml medium was added per well. On days three and five, cells were split 1:1 in fresh culture medium. After seven days, viable cells were extracted using density gradient centrifugation. Cells were resuspended, pooled, and carefully layered on top of 5 ml Histopaque®-1119 (Merck) in a 50 ml centrifugation tube (Sarstedt). After centrifugation at 850 g for 7 minutes, the cell layer between Histopaque and medium was collected and transferred to another tube containing 15 ml fresh medium. The suspension was centrifuged at 350 g for 5 minutes and the pellet was resuspended in medium, then cells were counted and seeded into a 24-well plate at a concentration of 1 x 10^6 cells per ml. Antigen experienced cells were used on days eight to ten.

2.4. Single molecule tracking

Bilayers were equipped with IE^k/MCC or IE^k/2b4_5CC7_2 peptide-MHCs, which had been labeled with either Alexa Fluor 647 (AF647, Thermo Fisher Scientific) or Abberior STAR 635P (Abberior, Germany). Wells featuring fluorophores at densities low enough to detect single molecule events but sufficient to guarantee an adequate number of events were selected for imaging. After adding cells suspended in imaging buffer to the wells, cells interacting with the bilayer were identified by white-light interference reflection microscopy (IRM) and placed into a region of interest (ROI) of 150 x 150 pixels. The cells were imaged using a 642 nm laser (Coherent). Images were taken in TIRF mode over a period of a few minutes with delays between acquisitions (time-lags) differing in length: 512 ms, 1025 ms, 2050 ms, 4100 ms, or 8200 ms. Samples were illuminated for 250 ms, with laser power density set to around 14 – 16 W/cm^2 for experiments with Abberior STAR 635P and 4 – 5 W/cm^2 for AF647. Images were acquired with an exposure time of 400 ms. The acquired raw .tif image stacks of 200 – 1000 pictures were analyzed using the open-source image processing software ImageJ. Single molecule binding events are characterized by a severe reduction in fluorophore mobility. This allows for determination of the length of binding events by counting the number of frames for which a fluorophore stays in place by eye and multiplying that number with the corresponding

time-lag. This was done for a statistically relevant number of binding events (around 150 – 200 events) for each time-lag. Binding lifetimes were recorded and used for statistical analysis.

2.5. Fluorophore lifetime measurements

For determination of the bleaching constants of AF647 and Abberior STAR 635P, high density immobile lipid bilayers were used. A unilamellar lipid vesicle solution containing 1 % Ni-DGS NTA and 99 % 1,2-dioleoyl-sn-glycero-3-phosphocholine (DPPC, Avanti polar lipids) was diluted 1:5 in 1x PBS and applied to a 16-well-chamber at 60 °C. Lipids were added in three aliquots of 40 µl each with incubation periods of 5 minutes between each step for a total incubation time of 15 minutes. Bilayers were then washed with 1x PBS and supplemented with the respective I-E^k/peptide complex at concentrations of 50 – 100 ng per well.

Microscopy was carried out with the same setup as used for single molecule tracking. Wells with sufficient densities were selected and bilayers were imaged in imaging buffer using the same time-lags between acquisitions as interaction lifetime experiments.

2.6. Single molecule FRET

T cells (0.25 x 10^6) were centrifuged at 350 g for 5 minutes and resuspended in 50 µl imaging buffer, then stained with 10 µg/ml H57 anti-TCR antibody single chain fragment (H57 scF_V, produced as published in Huppa et al., 2010) for 20 minutes on ice. For TCR labeling, 1 part Alexa Fluor 555-bound H57 scF_V was mixed with 9 parts unlabeled H57 scF_V prior to staining, resulting in a fraction of 10 % of TCRs being labeled with AF555. After staining, cells were washed into imaging buffer and kept on ice until imaging. Fresh cells were stained every 60 minutes.

Bilayers were equipped with ICAM-1, B7-1 and IE^k/peptide complexes labeled with the acceptor fluorophore AF647. Cells were added to the bilayer and single cells were placed into a ROI of 200 x 200 pixels. The TCR-bound donor fluorophores were excited with a 532 nm laser in TIRF mode for 20 ms with a power density of 0.10 kW/cm^2. Images were taken in the donor and acceptor channels with several time-lags between acquisitions: 84 ms, 252 ms, 476 ms, 923 ms, 1820 ms, or 3640 ms. The resulting raw .tif image stacks were analyzed using ImageJ. Binding event length was determined by counting the number of frames for which a signal appeared in the acceptor channel and multiplying that number with the corresponding

time-lag between acquisitions. This was done for a statistically relevant number of events per time-lag (150 – 200 events) and recorded for statistical analysis.

2.7. Bulk FRET measurements

Bulk FRET measurements were conducted using the same setup as single molecule FRET imaging experiments. T cells were stained in 50 µl cell culture medium with AF555-H57 scF_V at concentrations higher than 5 µg/ml for 20 minutes, ensuring labeling rates approaching 100 %. Cells were allowed to settle on lipid bilayers equipped with ICAM-1, B7 and high densities of AF647-IE^k/peptide for 2 minutes. Single cells were placed inside a ROI of 200 x 200 pixels using the 532 nm laser at the lowest possible power setting to avoid photobleaching. Imaging was performed in FRET donor and acceptor channels with the following protocol: First, a AF647 acquisition (642 nm laser, 1 W/cm^2), then a AF555/FRET acquisition (FRET before photobleaching, 532 nm laser at 10 W/cm^2), followed by a high-power 642 nm bleach pulse (2000 W/cm^2), a second AF647 acquisition (to confirm sufficient acceptor bleaching, 1 W/cm^2), and finally another AF555 acquisition (to record donor recovery, 10 W/cm^2). Illumination time was set to 30 ms for all acquisitions. For calculation of FRET yields, donor recovery after photoreceptor bleaching (DRAAPB) was determined using a custom script in MatLab R2022a (MathWorks, USA), as previously described (Huppa et al. 2010). Donor and acceptor channel were superimposed using an image of fluorescent beads as a reference for spatial alignment. Camera background was subtracted from the raw pixel intensities in each picture. Afterwards, AF555 intensity before acceptor photobleaching (DD_{pre}) was subtracted from the AF555 intensity after bleaching (DD_{post}), which was then divided by DD_{post} to obtain the FRET yield.

$$FRET\ yield = \frac{DD_{post} - DD_{pre}}{DD_{post}}$$

Ligand densities were calculated by dividing mean raw intensities of SLB (AF647) acquisitions by the intensity of single molecule fluorophore emissions, subtracting the camera background and multiplying with the conversion factor 39.06 (converting molecules per pixel to molecules/µm^2).

2.8. Statistical analysis of TCR-pMHC interaction lifetimes

Statistical analysis was performed in Prism 9 (GraphPad, USA). Interaction lifetimes recorded from single molecule tracking and single molecule FRET experiments were compiled and converted to an inverse cumulative decay function. The values were then divided by the total number of traces recorded for normalization. The resulting lifetime distributions were fitted with a single-phase exponential decay to obtain the apparent interaction lifetimes ($\tau = 1/k$). Both tracking and FRET methods are susceptible to photobleaching dependent on the number of acquisitions, as well as the implemented illumination time and power density. Therefore, to calculate exact values for interaction half-lives, correction for photobleaching is needed.

For calculating the bleaching rate constant (k_{bleach}) and then corrected interaction half-lives, two methods were used. Fluorescence lifetime measurements were conducted as described previously in parallel to single molecule tracking experiments. For each resulting raw .tif stack, mean fluorophore intensity for each acquisition was calculated using ImageJ. We then calculated the mean emission intensity per μm^2, which was corrected for background. The resulting values were fitted to a single-phase decay function in Prism, yielding k_{bleach} for each recorded time-lag. Binding lifetime results were then adjusted according to the formula

$$k_{off} = k_{apparent} - k_{bleach}$$

for each recorded time-lag, with $t_{off} = \frac{1}{k_{off}}$.

For the second correction method, tracking and FRET experiments were performed using at least three different time-lags. Binding lifetime distributions were plotted against the number of frames events were visible for and fitted with a single-phase decay function in Prism. The resulting apparent lifetimes were then plotted against the respective time-lags and fitted according to the function

$$f(x) = t_{off} / ((t_{off} / bleach) + x),$$

which gave us the bleach corrected interaction lifetime (t_{off}).

All t_{off} were converted to interaction half-lives using the formula

$$t_{1/2} = t_{off} * \ln(2).$$

3. Results

3.1. Determination of ligand affinities using bulk FRET

We first determined the synaptic FRET yield of T cell – ligand interactions according to the methodology set forth by Huppa et al. (Huppa et al. 2010). For this, we employed T cells isolated from the spleens and lymph nodes of 5c.c7 TCR transgenic mice. We allowed antigen experienced T cells to interact with two different ligands presented on the MHC II molecule I-E^k: the moth cytochrome C peptide 88-103 (MCC) and the 2b4_5CC7_2 peptide. Ligand peptides were conjugated with Alexa Fluor 647 (AF647) at their C-terminus, serving as a FRET acceptor. I-E^k-peptide complexes were presented on a planar functionalized SLB, which allow for rapid lateral diffusion and random distribution of surface proteins and hence reflect many of the properties of an APC-surface. In our case, SLBs were equipped with the adhesion molecule ICAM-1, the costimulatory peptide B7-1, and several different densities of I-E^k presenting the respective ligand peptide. T cells were stained with a H57 scF_v, which was site-specifically labeled with Alexa Fluor 555 (AF555), acting as a FRET donor. The distance between fluorophores allows measurable FRET between donor and acceptor fluorophore to only occur while TCRs actively engage pMHCII molecules (Huppa et al. 2010). Acquisitions of whole cells were taken before and after photobleaching of the acceptor fluorophores, and mean intensities of the pre- and post-bleaching images were converted to FRET yield in form of donor recovery after acceptor photobleaching (DRAAPB, Figure 2; for details see methods section). The maximal FRET yield that can be reached depends on the FRET efficiency of the employed fluorophores and their distance in the TCR – pMHC bound state. Previous studies have placed FRET efficiency of 5c.c7/H57-AF555 and I-E^k/MCC-AF647 at about 78 % which hence amounted to the highest FRET yield value that we could expected for FRET-pair in question (Platzer 2019).

For I-E^k/MCC, the mean FRET yields were surprisingly low, with values of under 20 % at the highest ligand densities employed. Interaction with I-E^k/2b4_5CC7_2-equipped SLBs showed considerably elevated FRET yields of around 50 %. These results suggest that I-E^k/2b4_5CC7_2 exhibits a particularly high affinity when engaged by the 5c.c7 TCR.

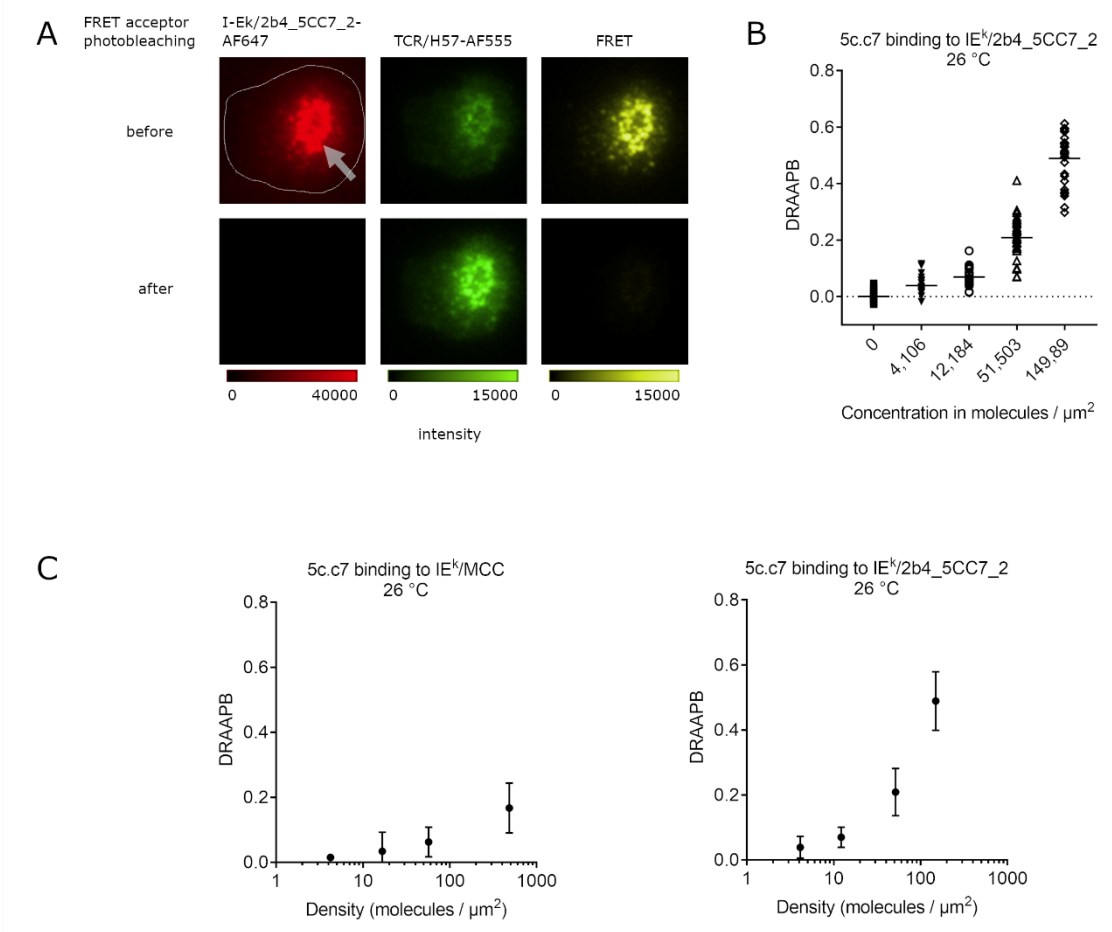

Figure 2: Bulk FRET measurements
A) Bulk FRET imaging acquisitions of a 5c.c7 TCR transgenic T cell interacting with a I-E^k/2b4_5CC7_2-functionalized SLB, showing a pronounced cSMAC (indicated by the arrow). TCRs were stained with an Alexa Fluor 555-conjugated H57 scF$_V$s., while pMHCs were labeled at with Alexa Fluor 647 via a linker fused to the C-terminus of the presented peptide. Images were acquired for both the donor (AF555) and acceptor (AF647) channels before and after bleaching of AF647 with the use of a high-powered red laser pulse. FRET, as depicted in the upper right panel, was detected in the FRET acceptor channel upon excitation of the FRET donor. Note that the disappearance of any signal in the FRET acceptor and FRET channel after bleaching coincides with an increase in intensity in the FRET donor channel (DRAAPB), which is a consequence of abrogated energy transfer due to the absence of a receptive FRET acceptor. (Created with BioRender.com) **B)** DRAAPB values for 5c.c7 TCR transgenic T cells stained with H57 scF$_V$-AF555 engaging SLBs with several densities of I-E^k/2b4_5CC7_2. Mean values were calculated from a minimum of 30 cells for each condition. Imaging was performed at 26 °C. **C)** Mean DRAAPB values with standard deviations plotted against the ligand densities they were recorded at for I-E^k/MCC and I-E^k/2b4_5CC7_2.

3.2. Determination of interaction half-lives via smFRET

Next, we determined interaction half-lives using a single molecule FRET (smFRET) based assay which allows for quantification of TCR – pMHC interactions *in situ* (Huppa et al. 2010). This method enabled us to track single molecule TCR – pMHC binding events over time and determine the length of these interactions with high temporal resolution. Prior to imaging, around 10 % of TCRs on 5c.c7 TCR transgenic T cells were stained with H57 scF_v-AF555 serving as the FRET donor. Stained cells were confronted with SLBs carrying I-E^k/MCC-AF647 or I-E^k/2b4_5CC7_2-AF647 at low densities, making it possible to detect single fluorophore FRET events after excitation of the donor. Serial rebinding of a pMHC from a labeled to an unlabeled TCR results in disappearance of the FRET signal due to the absence of a donor fluorophore (Figure 3A). Measured interaction lifetimes would therefore mostly reflect single binding events given the exceedingly low probability of recording serial rebinding within the chosen imaging setting.

Engagement of the SLB by T cells is followed by fast recruitment of I-E^k to the immunological synapse and formation of a cSMAC, especially when using the higher affinity 2b4_5CC7_2 ligand. This made it more challenging to clearly discern smFRET events due to increased cross-excitation of the acceptor fluorophore, as well as bleed-through of donor emission light into the acceptor channel and an overall increase in FRET events. We therefore only imaged cells in the early stages of SLB engagement, which had not yet given rise to distinguished cSMACs. Imaging was performed by streaming acquisitions using total internal reflection fluorescence (TIRF) microscopy with short exposure times (30 ms) and laser illumination power densities of 100 W/cm^2, minimizing photobleaching while still allowing for clear identification of diffraction-limited single molecule FRET events in the analysis. Binding lifetimes were determined by analyzing the length of events in the FRET acceptor channel (Figure 3D). During the experiments, we noticed frequent artifacts presumably produced by vesicles inside the T cell, the number of which could be reduced by increasing the TIRF angle employed at the microscope.

Both the donor and the acceptor fluorophore are prone to photobleaching, an effect, which is proportional to power density of the employed lasers used for excitation and the illumination time. Since photobleaching of a fluorophore is a stochastic event, it can be corrected for as part of the analysis by determining a bleaching rate constant (k_{bleach}). We hence traced FRET events caused by TCR – pMHC interactions with the use of different time-lags between acquisitions and then fitted the recorded data with an exponential decay model, each of which

provided us with a combination of k_{bleach} and k_{off}. Since the rate of bleaching depended on the number of acquisitions only and TCR-pMHC unbinding on the time passed between acquisitions, we were able to separate k_{bleach} from k_{off} or the lifetime τ (for further details please refer to the methods section).

Shown in Figure 3C are the mean half-lives for 5c.c7 TCR interactions with I-E^k/MCC and I-E^k/2b4_5CC7_2 at room temperature and 37 °C. Interactions with MCC as a ligand were typically short, with an average half-live of 3.3 seconds at room temperature and 1.52 s at 37 °C. This is consistent with the results of a previous study by Huppa et al., although they measured even shorter half-lives with only 1.68 s at 24 °C (Huppa et al. 2010). Binding lifetime measurements with I-E^k/2b4_5CC7_2 resulted in considerably higher half-lives of 14.2 s at room temperature and 9.9 s at 37 °C.

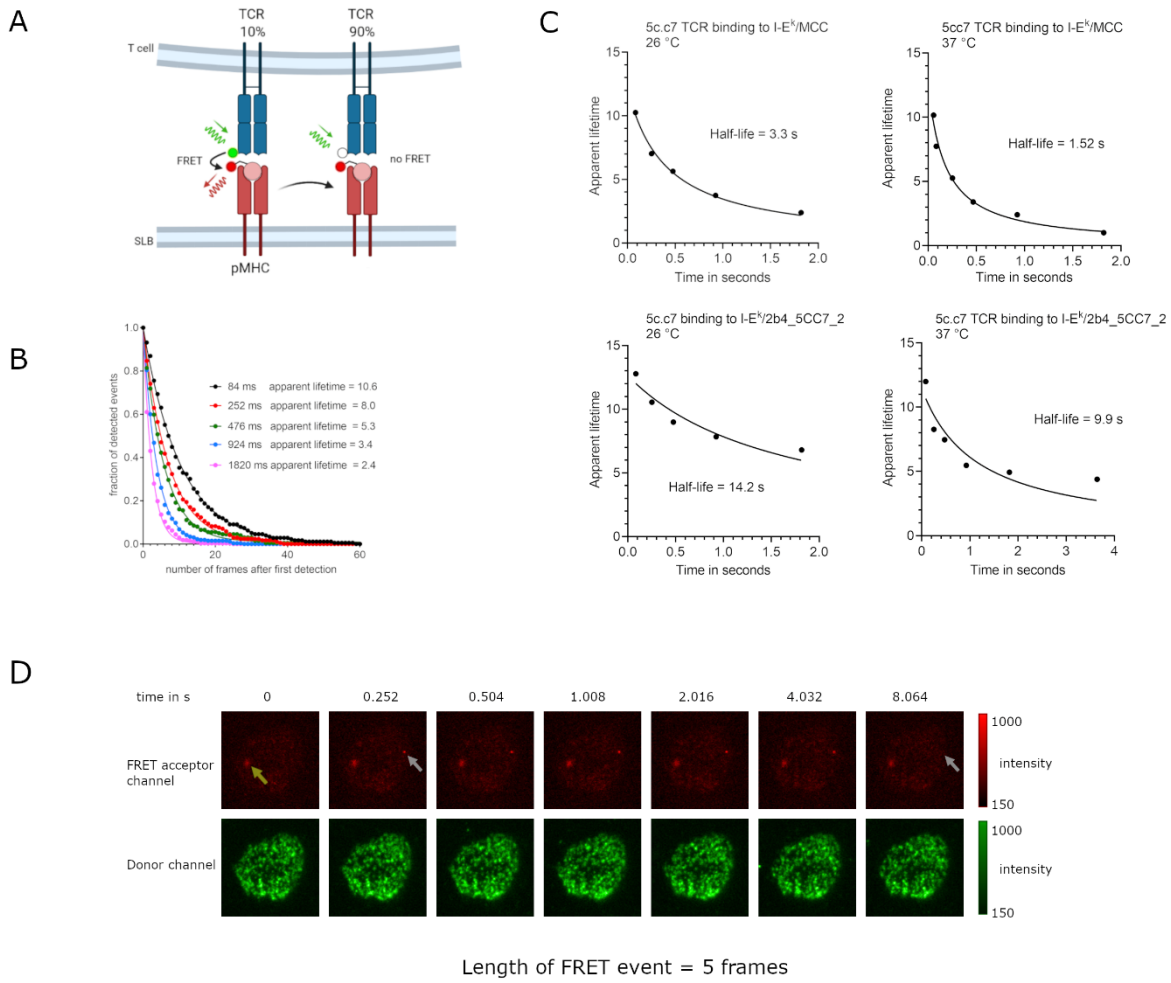

Figure 3: Determination of binding lifetimes of the 5c.c7 TCR to the ligands I-E^k/MCC and I-E^k/2b4_5CC7_2 via smFRET.

A) Scheme of a 5c.c7 TCR transgenic T cell interacting with its nominal antigen I-E^k/MCC displayed on a protein-functionalized supported lipid bilayer (SLB). Cells interacting with the SLB were imaged using a 532 nm laser for excitation in TIRF microscopy configuration. About 10 % of TCRs were labeled with H57 scF_v site-specifically conjugated with AF555, while all pMHCs were decorated with AF647 at the C-terminus of the presented peptide. In case both interacting TCR and pMHC were conjugated with their respective fluorophore, the distance between them (4.1 nm) would be small enough for FRET to occur. Once the pMHC rebinds a different, unlabeled TCR, no FRET takes place due to the absence of a donor fluorophore. (Created with BioRender.com) **B)** Example for the statistical analysis of recorded single molecule FRET events to arrive at binding lifetimes. The relative number of observed single molecule FRET events was plotted against the number of time frames during which the events appeared for five to six chosen time-lags. The data were then fitted to a single exponential decay (colored lines). Apparent lifetimes were calculated for each time lag. Dwell time distributions were calculated from the analysis of >150 trajectories for each time lag. **C)** Charts showing apparent lifetimes (a function of k_{off} and k_{bleach}) plotted against the time-lags as they had been selected for recording the single molecule FRET-traces for indicated 5c.c7 TCR-pMHC interactions and temperatures. **D)** Example of a FRET trace recorded over a period of ~8 seconds. The FRET signal (indicated by the white arrow) appeared in the second frame in the acceptor channel (top) and disappeared within a single frame, making it possible to calculate the duration of FRET and therefore the length of the binding interaction. The yellow arrow indicates an artifact presumably resulting from am intracellular vesicle. The donor channel (bottom) shows the signal of donor fluorophores bound to TCRs on the T cell within the same period.

3.3. Determination of lifetimes via single molecule tracking

Next, we followed a single molecule tracking based approach, which has been established as another method to measure interaction lifetimes between TCRs and pMHCs *in situ* (O'Donoghue et al. 2013, Lin et al. 2019). For direct data comparison we employed 5c.c7 TCR transgenic T cells to investigate TCR binding kinetics with I-E^k/MCC and I-E^k/2b4_5CC7_2. The stimulatory peptides complexed with I-E^k were C-terminally conjugated with Abberior STAR 635P, which was reported by the manufacturer a particularly photostable fluorophore, which we confirmed by means of quantitative bleaching experimentation (Figure 4C). Here experiments were performed with the use of immobile SLBs featuring fluorescence-tagged pMHC at high densities, which were imaged applying a streaming acquisition protocol with varying time-lags (for details please refer to the methods section).

For TCR – pMHC binding lifetime measurement experiments, I-E^k densities on the bilayer were kept low in order to easily identify single molecule binding events. Prior to T cell imaging, bilayer fluidity was assessed with a single fluorophore bleaching step and subsequent evaluation of the time needed for repopulation of the according area with pMHCs. The bilayer was also examined for artifacts in form of pMHC immobilizations, which would constitute background noise in the analysis. T cells were allowed to settle on the SLBs equipped with ICAM-1, B7-1 and pMHCs labeled with Abberior STAR 635P. T cells were imaged using a 642 nm laser with a comparatively low-power illumination (250 ms, 15 W/cm^2) and long exposure times (400 ms) to avoid unnecessary photobleaching. Under these conditions, unbound, fast-moving pMHCs appeared blurry in acquisitions, while the TCR-bound, slow-

moving faction was visible as defined bright dots (Figure 4F). Acquisitions were streamed over a time of several minutes per cell with two different time-lags between images for each run. Lifetime measurements obtained by single molecule tracking depend on the employed time-lag, mainly due to increased photobleaching when using short delays. Long delays on the other hand result in a loss of temporal resolution, so we aimed for reaching a middle-ground to arrive at reliable results.

With single molecule tracking measurements, potential rebinding would not be visible beyond possible slight shifts in location of the bound pMHC between acquisitions. Interactions comprised of several sequential binding events would therefore be recorded a one longer binding event, which distinguishes results obtained by this method from those recorded using smFRET (Figure 4A).

Half-lives calculated with tracking were typically longer than those recorded with smFRET, with TCR – I-E^k/MCC-interactions being in the range of approximately 3.5 – 4 s at 26 °C and 1.6 – 1.9 s at 37 °C, and TCR – I-E^k/2b4_5CC7_2-interactions in the range of 14.8 – 19.1 s at 26 °C and 10.3 – 12.3 s at 37 °C (Figure 4D, E). However, fitting interaction lifetime distributions to the single exponential decay functions turned out unsatisfactory even though all R^2 were in acceptable ranges (>0.9). We identified the underlying complication in a significant number of long-dwelling events the existence of which could not be explained by our initial assumptions.

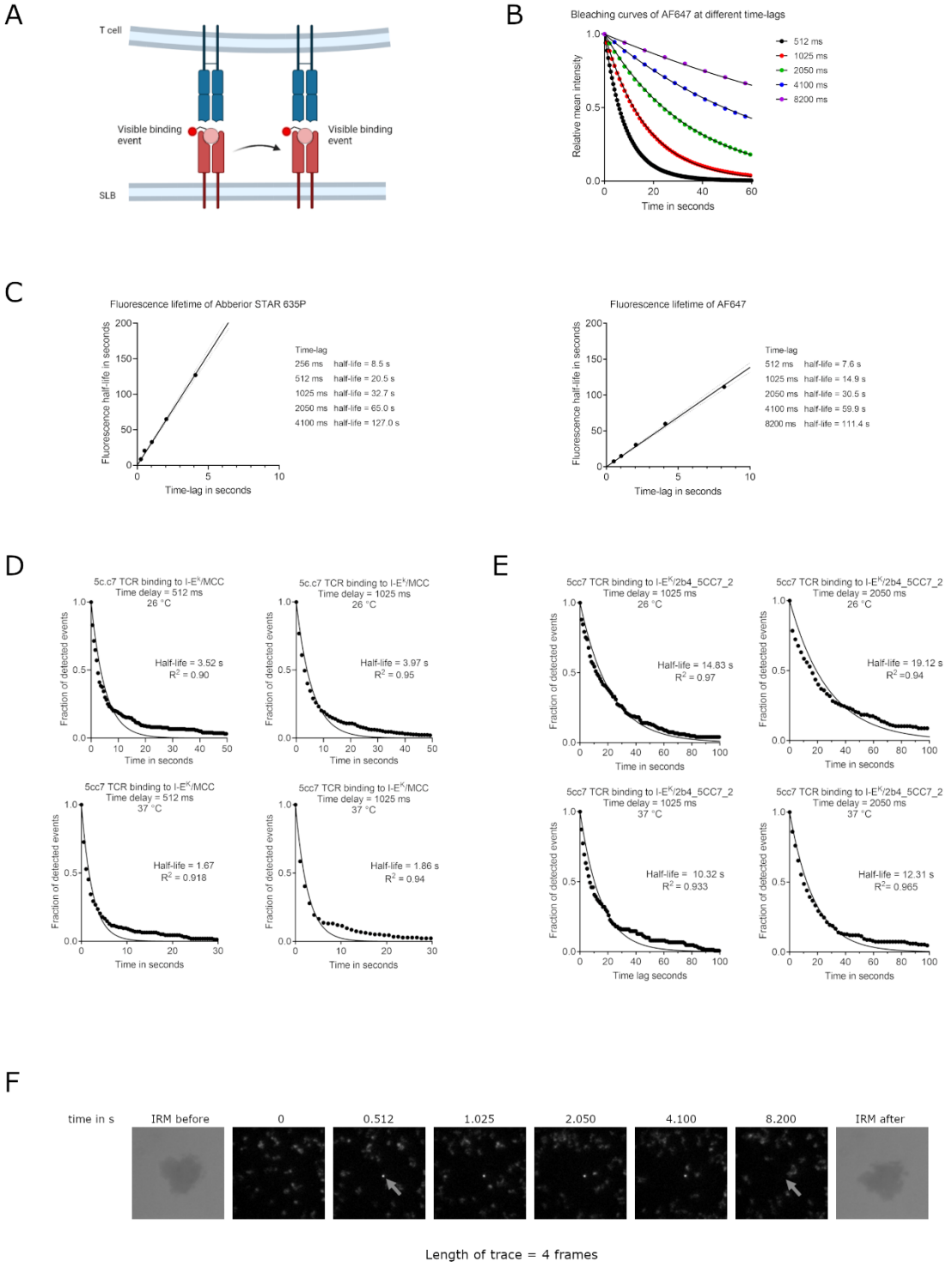

Figure 4: Determination of binding lifetimes of the 5c.c7 TCR to the ligands I-E^k/MCC and I-E^k/2b4_5CC7_2 via single molecule tracking.

A) Scheme of the TCR of a 5c.c7 transgenic T cell interacting with the pMHCs presented on a functionalized supported lipid bilayer (SLB). Unbound pMHCs (labeled with the fluorophore Abberior STAR 635P or AF647) move freely on the lateral plane until engaged by a TCR, at which point the speed of diffusion is severely reduced. T cells engaging the SLB were imaged in TIRF mode using a red laser with long exposure times (400 ms). This results in

unbound, fast-moving pMHCs being blurry in the acquired images, while TCR-bound, slow-moving pMHCs are visible as well-defined spots. Rebinding of a pMHC to another TCR would be recorded as one longer binding event using this method. **B)** Example of fluorescence lifetime measurements recorded for AF647 at five different time-lags. Relative mean intensities were plotted against the acquisition time (colored dots) and fitted with a single-phase exponential decay (black lines). **C)** Plots of fluorescence half-lives of Abberior STAR 635P and AF647 for each time-lag. Excitation light intensity was set to 15 W/cm^2 for Abberior STAR635P and 5 W/cm^2 for AF647, ( ) at which fluorophore emission intensity was at the lower limit of good visibility for binding events. Fluorescence half-lives were plotted against their respective time-lags. **D, E)** Dwell time of interactions of 5c.c7 TCRs with I-E^k/MCC-STAR 635P (D) and I-E^k/2b4_5CC7_2-STAR 635P (E) recorded by single molecule tracking at 26 °C and 37 °C. Decay plots were fitted to single-phase exponential decay curves (black lines). Each experiment was performed using two different time-lags, which were adjusted for the expected interaction lengths of the respective ligand (512 ms and 1025 ms for MCC, 1025 ms and 2050 ms for 2b4_5CC7_2). The calculated lifetimes (t_{off}) were converted to interaction half-lives ($t_{1/2}$), which are shown here. Dwell time distributions were calculated from the analysis of >150 trajectories for each time lag **F)** Example of a binding event recorded over a period of around 8 seconds using the setup described above. Before and after fluorescence imaging, a picture of the imaged cell was taken using interference reflection microscopy (IRM) to approximate the location of the cell during imaging. Events typically become visible and disappear within a single frame, making it possible to count the number of frames the fluorophore stays in place and calculating the lifetime of the interaction.

3.4. Tracking experiments with the 5c.c7 TCR binding to a null ligand revealed potential unspecific binding interactions by Abberior STAR 635P

A possible explanation for the substandard fit of the tracks to a single exponential function consisted in unspecific binding of the fluorophore we had employed. We considered this to be plausible, especially in the absence of any published studies involving the use of Abberior STAR 635P for the investigation of TCR – pMHC-interactions. To test this possibility, we took advantage of a null ligand which is known not to interact with the 5c.c7 TCR. Any recorded fluorophore immobilizations of such ligands would directly invoke non-specific binding, which would next need to be prevented or accounted for to arrive at robust analyses. Null ligand tracking experiments were hence performed with the setup described above, using I-E^k/MCC-STAR as a positive control and a way to compare and quantize the number of recorded immobilizations of I-E^k/null-STAR 635P. Results of the lifetime analysis are shown in Figure 5A. After cells were added, immobilizations were recorded for both I-E^k/null and I-E^k/MCC at room temperature from eight cells each. Comparing interaction frequency distributions for both ligands, we did in fact see a considerable number of apparent binding events with the null ligand. These events were apparently randomly distributed, not only localized in area covered by T cells as assessed by IRM acquisitions done in parallel. These observations rendered it highly likely that such immobilizations had resulted from fluorophore interactions with the SLB and not from specific TCR-interactions. Since the calculated half-life amounted to 5.56 s for the null-ligand, we considered it likely that the previously measured

half-life of 3.34 second for I-E^k/MCC was in fact to long and skewed by a considerable number of unspecific pMHC immobilizations on the SLB.

To avoid this complication altogether we repeated the tracking experiments with the use of AF647-labeled null ligands (Figure 5B). Again, interaction lifetime distributions were compared to those recorded from interactions with I-E^k/MCC, also labeled with AF647. For I-E^k/null-AF647, the number of immobilization events was in the expected range, with the few immobilizations recorded typically being rather short. These findings confirm the notion that the high number of immobilizations recorded with the null ligand were in fact due to unspecific interactions of the fluorophore STAR 635P after adding cells. This led us to conduct all further tracking experiments with the use of AF647-labeled ligands, in spite of the fluorophore's considerably higher photosensitivity.

3.5. Single molecule tracking measurements with the use of AF647-labeled TCR-ligands

The relatively high photosensitivity of AF647 rendered it necessary to correct for photobleaching as a means to arrive at robust lifetimes. For this, we employed the same correction method we had already used for the analysis of the smFRET-based experiments. To this end we recorded traces at several time-lags back-to-back and fitting obtained apparent (uncorrected) lifetimes to a model providing us with a bleaching constant and the corrected lifetimes.

In Figure 5C, lifetime results from 5c.c7 TCR interactions with I-E^k/MCC recorded with smFRET at 26 °C are contrasted with tracking observations using I-E^k/MCC-AF647 at 26 °C. The bleach corrected mean half-life measured by single molecule tracking was determined to be 7.72 s. Comparing this to the mean half-life of 3.3 s measured with smFRET (also see Figure 3C), it is apparent that tracking lifetime measurements yield considerably increased interaction times. This implies the existence of pMHC rebinding to several TCRs, which is only recorded with the tracking method and would increase observed lifetimes vis-à-vis smFRET-based measurements. The extent of this effect and therefore the amount of rebinding taking place can however not be inferred from these results alone and will require further analytic approaches requiring Monte-Carlo-based simulation.

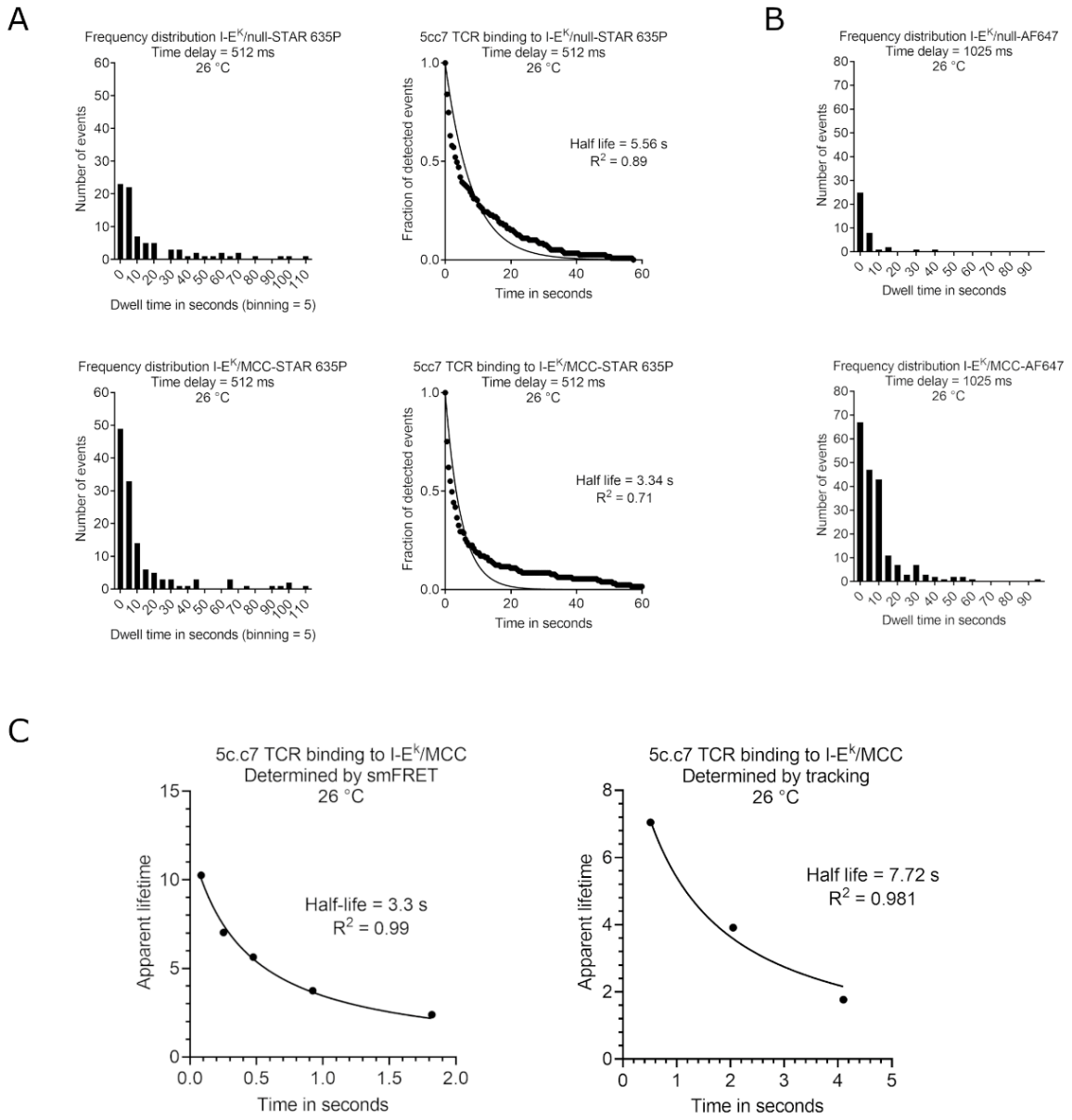

Figure 5: Comparison of lifetime data derived from smFRET experiments to data from single molecule tracking experiments

A) Results of single molecule tracking experiments with the 5c.c7 TCR binding to I-E^k/null and I-E^k/MCC labeled with Abberior STAR 635P. Histograms show the binding lifetime distribution of the total number of observed events using the null ligand (top left) and MCC (bottom left) acquired from 8 cells each. Decay plots with single phase exponential decay fit (black lines) show the half-lives of immobilizations observed when applying the null ligand (top right) and MCC (bottom right). Experiments involving these ligands were performed on the same day and using the same experimental setup. **B)** Histograms showing the binding lifetime distribution of 5c.c7 to I-E^k/null and I-E^k/MCC labeled with AF647. Both experiments were performed on the same day with 2 cells recorded and with the same experimental setup. **C)** Charts showing apparent interaction lifetimes of 5c.c7 binding to I-E^k/MCC-AF647 determined by smFRET (left), and single molecule tracking (right) plotted against the respective time-lags. The plots were fitted, and interaction lifetimes were corrected for photobleaching. Half-lives corrected for bleaching are shown. Experiments were performed at 26 °C.

4. Discussion

Even though much progress has been made in revealing the molecular mechanisms underlying T-cell antigen recognition in the past few years, the question of how TCRs achieve their striking antigen sensitivity despite low antigen affinities and an overall abundance of non-activating pMHCs has been left unanswered. The idea of serial rebinding of single pMHCs to several TCRs has been proposed as an explanation to this problem for almost 30 years but has not been verified since. To investigate the possibility of rebinding playing a role in T-cell activation, we have employed minimally invasive live cell fluorescence microscopy. This approach has made it possible to detect and quantify TCR – pMHC interactions with high spatial and temporal resolution and without affecting cellular integrity.

Overall, our results imply the existence of serial rebinding in TCR – pMHC interactions between T cells and APCs in the context of the immunological synapse. Single molecule tracking experiments for 5c.c7 TCRs binding to I-E^k/MCC-AF647, which register rebinding events in their lifetime distributions, resulted in half-lives of more than double the length of smFRET measurements for the same interaction. It can therefore be assumed that at least a fraction of pMHCs binds at least two TCRs sequentially. Although one cannot infer the size of this fraction or the number of TCRs serially engaged by single pMHCs from these results alone, it is evident that this behavior could influence T-cell activation kinetics and could even be part of the reason underlying the remarkable sensitivity of T cells.

Bulk FRET analysis revealed that FRET yield and therefore TCR occupancy is higher for I-E^k/2b4_5CC7_2 than I-E^k/MCC within the immunological synapse. Together with the fact that I-E^k/2b4_5CC7_2 interaction half-lives were considerably longer than the half-lives of I-E^k/MCC, this indicates that 2b4_5CC7_2 is a particularly high affinity ligand to the 5c.c7 TCR. In previous studies, 5c.c7 TCR reactive H57 antibody single chain fragments have been used as high affinity ligands to study T-cell activation *in situ* (Hellmeier et al. 2021). However, scF_Vs have the disadvantage of not having the same TCR binding site as physiological ligands and therefore possibly activating TCRs in an alternate manner when compared to pMHCs. Intracellular TCR/CD3 phosphorylation kinetics after antibody binding have not yet been sufficiently characterized and could differ substantially from those after pMHC-engagement. Since TCR binding kinetics and T-cell activation mechanisms have been a focus point for many studies, employing a physiological ligand featuring a high affinity instead of a scF_Vs might yield more informative and conclusive findings. Our results indicate that 2b4_5CC7_2 might be a

suitable alternative for this purpose. The difference between tracking and smFRET data appeared smaller for interactions of 5c.c7 with I-E^k/2b4_5CC7_2 than I-E^k/MCC-AF647, as inferred from measurements with Abberior STAR 635P. Combined with the previously published observation that distances between single high-affinity TCR – ligand pairs cannot exceed 20 nm (Hellmeier et al. 2021), this implies the role of rebinding in T-cell activation to be smaller for high-affinity ligands, although the rebinding cannot be ruled out.

The length of interaction lifetimes of I-E^k/2b4_5CC7_2 we measured has practical implications for future single molecule lifetime tracking experiments. Since the amount of photobleaching is a factor of total illumination time, short time-lags between acquisitions result in faster bleaching of the fluorophores. At 26 °C, the interaction half-life of 5c.c7 binding to I-E^k/2b4_5CC7_2 approached 20 s when determined by single molecule tracking with a time-lag of 2050 ms. The fluorescence half-life of AF647 using this time-lag was determined to be only 30.5 s, meaning that a considerable portion of immobilized fluorophores might be bleached before unbinding occurs. This is especially unfavorable for the detection of longer binding events, which have a significantly higher chance of bleaching before unbinding. Thus, to make sure that the determined lifetimes are representative of TCR – pMHC off-rates rather than fluorophore photobleaching, it might be more appropriate to employ longer time-lags in the range of 5 – 8 s. This would guarantee that at least a portion of long-dwelling events can be recorded.

In the course of the single molecule tracking experiments we conducted using the fluorophore Abberior STAR 635P as a label for I-E^k/MCC and I-E^k/2b4_5CC7_2, we noticed that lifetime distributions did not fit the single-phase decay model we assumed for binding lifetimes. This was found to be an effect of non-specific ligand interactions with the T-cell plasma membrane, since we failed to detect these interactions prior to adding the T cells to the bilayer, which also led us to rule out artifacts in the bilayer itself as a possible cause. In experiments with a TCR-nonbinding null ligand, these interactions in form of fluorophore immobilizations were visible when using Abberior STAR 635P-bound pMHCs but not with ligands coupled to AF647, confirming that they had indeed been caused by the fluorophore itself. Immobilizations were not confined to the areas under bilayer-interacting cells but seemingly appeared randomly in observed ROIs. The best explanation is hence that Abberior STAR 635P interacts with some constituents of the T-cell membrane other than the TCRs, since T cells are known to spread and form protrusions on surfaces after antigen contact (Pettmann et al. 2018), while TCRs are mostly localized centrally under the main body of the cell. Single molecule pMHC tracking does

not allow for differentiation between TCR – pMHC binding and other reasons for fluorophore immobilization. This renders Abberior STAR 635P unsuitable for *in situ* investigation of TCR – pMHC binding kinetics.

To comprehensively review the binding kinetics of the 5c.c7 TCR to I-E^k/MCC and I-E^k/2b4_5CC7_2, it is necessary to calculate on-rates of TCR – pMHC interactions in addition to off-rates/interaction lifetimes. Determination of on-rates could provide information regarding the likelihood of rebinding taking place for a certain receptor – ligand pair. High on-and off-rates can be expected to promote serial rebinding within the immunological synapse. Although the calculation of on-rates was outside the scope of this thesis, bulk FRET measurements conducted as part of this thesis could serve to determine dissociation constants (K_D) and together with the observed interaction lifetimes as a means to assess this parameter (Huppa et al. 2010), assuming the law of mass action to be true within the confines of the immunological synapse.

To fully understand the impact of serial rebinding on sensitized TCR – pMHC recognition and T-cell activation kinetics, the frequency and amount of rebinding within the immunological synapse must be determined. One method of doing this would be to perform a Monte-Carlo-based simulation for the influence rebinding would have on binding lifetime distributions. The resulting model could be used to predict how distributions would be altered by a certain fraction of pMHCs rebinding a certain number of times. By comparing this with the recorded distributions of binding durations, conclusions could be drawn about the importance of rebinding for sensitized antigen recognition of rare activating ligands and T-cell activation.

Abstract

T cells display remarkable sensitivity and specificity when recognizing stimulatory peptide-MHC complexes (pMHCs) on the surface of antigen presenting cells. How they accomplish this despite T-cell receptor (TCR) – pMHC interactions being of relatively low affinity is yet unknown. It has been hypothesized, that sequential rebinding of a single stimulatory pMHC to several TCRs may be a critical event in T-cell activation. We have employed two different single molecule fluorescence imaging methods: a single molecule tracking approach and a single molecule FRET based method. Binding interaction lifetimes were recorded with both methods, which were used to calculate TCR – MHC binding lifetime distributions and half-lives. Interestingly, we observed a two-fold increase in interaction half-lives when using the single molecule tracking approach, where we expected to record interaction lifetimes including rebinding. This leads us to conclude that binding of at least two TCRs by a single pMHC does occur, although the frequency of this behavior has yet to be determined. However, we propose that rebinding may be part of the reason underlying the high sensitivity of T cells to single ligand peptides.

Zusammenfassung

T-Zellen zeigen eine bemerkenswerte Empfindlichkeit und Spezifität bei der Erkennung von stimulierenden Peptid-MHC-Komplexen (pMHCs) auf der Oberfläche von Antigen-präsentierenden Zellen. Wie sie dies erreichen, obwohl die Wechselwirkungen zwischen T-Zell-Rezeptor (TCR) und pMHC von relativ geringer Affinität sind, ist noch unbekannt. Es wurde die Theorie aufgestellt, dass die sequenzielle Bindung eines einzelnen stimulierenden pMHC an mehrere TCRs ein kritisches Ereignis bei der T-Zell-Aktivierung sein könnte. Wir haben zwei verschiedene Einzelmolekül-Fluoreszenz-Imaging-Methoden angewandt: einen Einzelmolekül-Tracking-Ansatz und eine Einzelmolekül-FRET-basierte Methode. Mit beiden Methoden wurden die Lebensdauern der Bindungsinteraktionen aufgezeichnet, die zur Berechnung der Verteilung von TCR-MHC-Bindungsdauern und der Halbwertszeiten verwendet wurden. Interessanterweise beobachteten wir einen zweifachen Anstieg der Interaktionshalbwertszeiten bei Verwendung des Einzelmolekül-Tracking-Ansatzes, bei dem wir erwarteten, Interaktionslebensdauern einschließlich der seriellen Bindungen zu erfassen. Daraus schließen wir, dass die Bindung von mindestens zwei TCRs durch ein einzelnes pMHC vorkommt, obwohl die Häufigkeit dieses Verhaltens noch bestimmt werden muss. Wir vermuten jedoch, dass die sequenzielle Bindung ein Grund für die hohe Empfindlichkeit der T-Zellen gegenüber einzelnen Liganden ist.

List of abbreviations

AF647/555	Alexa Fluor 647/555
APC	Antigen presenting cell
CD4/CD8	Cluster of differentiation glycoprotein 4/8
cSMAC/pSMAC	Central/peripheral supra-molecular activation complex
DPPC	1,2-dioleoyl-sn-glycero-3-phosphocholine
DRAAPB	Donor recovery after acceptor photobleaching
FRET	Förster resonance energy transfer
IB	Imaging buffer
IL-2	Interleukin-2
IRM	Interference reflection microscopy
IS	Immunological synapse
MCC	Moth cytochrome C
MHC	Major histocompatibility complex
Ni-DGS NTA	1,2-dioleoyl-*sn*-glycero-3-[(N-(5-amino-1-carboxypentyl)iminodiacetic acid)succinyl] (nickel salt)
POPC	1-palmitoyl-2-oleoyl-sn-glycero-3-phosphocholine
ROI	Region of interest
scF_V	Antibody single chain variable fragment
SLB	Soluble lipid bilayer
smFRET	single molecule FRET
SPR	Surface plasmon resonance
TCR	T-cell receptor
TIRF	Total internal reflection fluorescence microscopy
TNFα	Tumor necrosis factor α

References

Ahmed R, Gray D. 1996. Immunological memory and protective immunity: understanding their relation. Science (New York, N.Y.), 272(5258):54–60.

Axmann M, Schütz GJ, Huppa JB. 2015. Measuring TCR-pMHC Binding In Situ using a FRET-based Microscopy Assay. Journal of Visualized Experiments, (104):53157.

Berney C, Danuser G. 2003. FRET or No FRET: A Quantitative Comparison. Biophysical Journal, 84(6):3992–4010.

Campi G, Varma R, Dustin ML. 2005. Actin and agonist MHC-peptide complex-dependent T cell receptor microclusters as scaffolds for signaling. The Journal of Experimental Medicine, 202(8):1031–1036.

Chen L, Flies DB. 2013. Molecular mechanisms of T cell co-stimulation and co-inhibition. Nature Reviews Immunology, 13(4):227–242.

Förster Th. 1948. Zwischenmolekulare Energiewanderung und Fluoreszenz. Annalen der Physik, 437(1–2):55–75.

Garcia KC, Degano M, Stanfield RL, Brunmark A, Jackson MR, Peterson PA, Teyton L, Wilson IA. 1996. An alphabeta T cell receptor structure at 2.5 A and its orientation in the TCR-MHC complex. Science (New York, N.Y.), 274(5285):209–219.

Grakoui A, Bromley SK, Sumen C, Davis MM, Shaw AS, Allen PM, Dustin ML. 1999. The Immunological Synapse: A Molecular Machine Controlling T Cell Activation. Science, 285(5425):221–227.

Harty JT, Tvinnereim AR, White DW. 2000. CD8+ T cell effector mechanisms in resistance to infection. Annual Review of Immunology, 18:275–308.

Hellmeier J, Platzer R, Eklund AS, Schlichthaerle T, Karner A, Motsch V, Schneider MC, Kurz E, Bamieh V, Brameshuber M, et al. 2021. DNA origami demonstrate the unique stimulatory power of single pMHCs as T cell antigens. Proceedings of the National Academy of Sciences, 118(4):e2016857118.

Huang J, Brameshuber M, Zeng X, Xie J, Li Q, Chien Y, Valitutti S, Davis MM. 2013. A Single Peptide-Major Histocompatibility Complex Ligand Triggers Digital Cytokine Secretion in CD4+ T Cells. Immunity, 39(5):846–857.

Huppa J, Davis M. 2013. The Interdisciplinary Science of T-cell Recognition. Advances in immunology, 119:1–50.

Huppa JB, Davis MM. 2003. T-cell-antigen recognition and the immunological synapse. Nature Reviews. Immunology, 3(12):973–983.

Huppa JB, Gleimer M, Sumen C, Davis MM. 2003. Continuous T cell receptor signaling required for synapse maintenance and full effector potential. Nature Immunology, 4(8):749–755.

Huppa JB, Axmann M, Mörtelmaier MA, Lillemeier BF, Newell EW, Brameshuber M, Klein LO, Schütz GJ, Davis MM. 2010. TCR–peptide–MHC interactions in situ show accelerated kinetics and increased affinity. Nature, 463(7283):963–967.

Irvine DJ, Purbhoo MA, Krogsgaard M, Davis MM. 2002. Direct observation of ligand recognition by T cells. Nature, 419(6909):845–849.

Kupfer A, Dennert G. 1984. Reorientation of the microtubule-organizing center and the Golgi apparatus in cloned cytotoxic lymphocytes triggered by binding to lysable target cells. Journal of Immunology (Baltimore, Md.: 1950), 133(5):2762–2766.

Lin JJY, Low-Nam ST, Alfieri KN, McAffee DB, Fay NC, Groves JT. 2019. Mapping the stochastic sequence of individual ligand-receptor binding events to cellular activation: T cells act on the rare events. Science Signaling, 12(564):eaat8715.

Litman GW, Rast JP, Fugmann SD. 2010. The origins of vertebrate adaptive immunity. Nature reviews. Immunology, 10(8):543–553.

van der Merwe PA, Dushek O. 2011. Mechanisms for T cell receptor triggering. Nature Reviews Immunology, 11(1):47–55.

Meuer SC, Acuto O, Hussey RE, Hodgdon JC, Fitzgerald KA, Schlossman SF, Reinherz EL. 1983. Evidence for the T3-associated 90K heterodimer as the T-cell antigen receptor. Nature, 303(5920):808–810.

Murphy K, Weaver C. 2016. Janeway's Immunonbiology. 9th edition 9th edition. New York London: GS Garland Science, Taylor & Francis Group.

O'Donoghue GP, Pielak RM, Smoligovets AA, Lin JJ, Groves JT. 2013. Direct single molecule measurement of TCR triggering by agonist pMHC in living primary T cells. eLife, 2:e00778.

Pettmann J, Santos AM, Dushek O, Davis SJ. 2018. Membrane Ultrastructure and T Cell Activation. Frontiers in Immunology, 9.

Platzer R. 2019. How Antigen is Presented to Sensitize T cells; a Molecular Imaging Approach. Medizinische Universität Wien.

Purbhoo MA, Irvine DJ, Huppa JB, Davis MM. 2004. T cell killing does not require the formation of a stable mature immunological synapse. Nature Immunology, 5(5):524–530.

Spiegel S, Kassis S, Wilchek M, Fishman PH. 1984. Direct visualization of redistribution and capping of fluorescent gangliosides on lymphocytes. The Journal of Cell Biology, 99(5):1575–1581.

Tseng S-Y, Waite JC, Liu M, Vardhana S, Dustin ML. 2008. T cell-dendritic cell immunological synapses contain TCR-dependent CD28-CD80 clusters that recruit protein kinase C theta. Journal of Immunology (Baltimore, Md.: 1950), 181(7):4852–4863.

Valitutti S, Müller S, Cella M, Padovan E, Lanzavecchia A. 1995. Serial triggering of many T-cell receptors by a few peptide-MHC complexes. Nature, 375(6527):148–151.

List of Figures